Neurotoxic lupus autoantibodies alter brain function through two distinct mechanisms

Thomas W. Faust[a], Eric H. Chang[a], Czeslawa Kowal[b], RoseAnn Berlin[a], Irina G. Gazaryan[a], Eva Bertini[b], Jie Zhang[b], Jorge Sanchez-Guerrero[c], Hilda E. Fragoso-Loyo[c], Bruce T. Volpe[a], Betty Diamond[b], and Patricio T. Huerta[a,1]

[a]Burke Cornell Medical Research Institute, Department of Neurology and Neuroscience, Weill Medical College of Cornell University, White Plains, NY 10605; [b]Autoimmune and Musculoskeletal Disease Center, Feinstein Institute for Medical Research, Manhasset, NY 11030; and [c]Department of Immunology and Rheumatology, Instituto Nacional de Ciencias Médicas y Nutrición Salvador Zubirán, México, Distrito Federal, México

Edited* by Matthew D. Scharff, Albert Einstein College of Medicine, Bronx, NY, and approved September 2, 2010 (received for review May 19, 2010)

Damaging interactions between antibodies and brain antigenic targets may be responsible for an expanding range of neurological disorders. In the case of systemic lupus erythematosus (SLE), patients generate autoantibodies (AAbs) that frequently bind dsDNA. Although some symptoms of SLE may arise from direct reactivity to dsDNA, much of the AAb-mediated damage originates from cross-reactivity with other antigens. We have studied lupus AAbs that bind dsDNA and cross-react with the NR2A and NR2B subunits of the NMDA receptor (NMDAR). In adult mouse models, when the blood–brain barrier is compromised, these NMDAR-reactive AAbs access the brain and elicit neuronal death with ensuing cognitive dysfunction and emotional disturbance. The cellular mechanisms that underlie these deleterious effects remain incompletely understood. Here, we show that, at low concentration, the NMDAR-reactive AAbs are positive modulators of receptor function that increase the size of NMDAR-mediated excitatory postsynaptic potentials, whereas at high concentration, the AAbs promote excitotoxicity through enhanced mitochondrial permeability transition. Other synaptic receptors are completely unaffected by the AAbs. NMDAR activation is required for producing both the synaptic and the mitochondrial effects. Our study thus reveals the mechanisms by which NMDAR-reactive AAbs trigger graded cellular alterations, which are likely to be responsible for the transient and permanent neuropsychiatric symptoms observed in patients with SLE. Our study also provides a model in which local AAb concentration determines the exact nature of the cellular response.

autoimmunity | mitochondrial stress | neuropsychiatric lupus | NMDA receptor

Systemic lupus erythematosus (SLE) is a chronic autoimmune disease that affects ~0.2% of the world's population, with up to 90% of the cases occurring in women of childbearing age (1, 2). The symptoms of SLE include arthritis, immunologic abnormalities, blood disorders, serositis, malar rashes, renal damage, skin rashes, and neurological disorders (3, 4). Use of immunosuppressive therapy, combined with antibiotic treatment that prevents the infectious complications of therapy, has extended the survival of SLE patients. However, as patients live longer, many develop abnormalities in either the central nervous system (CNS) or the peripheral nervous system that are collectively termed neuropsychiatric lupus (NPSLE) (5–7). The most common symptoms in NPSLE are cognitive impairment and emotional imbalance, which may have devastating consequences for the patient's quality of life. Additional CNS symptoms include anxiety, seizures, and psychosis.

SLE is characterized by the presence of autoantibodies (AAbs) that bind multiple self-antigens, although dsDNA has been identified as a major self-antigen, making dsDNA-reactive AAbs a diagnostic criterion for SLE (3, 4). Paradoxically, although some symptoms may arise from AAb reactivity to dsDNA, much AAb-mediated damage originates from cross-reactivity to other self-antigens (2). Clinical studies indicate that 40–50% of SLE patients carry AAbs that cross-react with dsDNA and NMDA receptors (NMDARs) (8–14). These AAbs are present in the blood but can also be found in the cerebrospinal fluid and brain parenchyma of some patients with SLE (8, 15–18). Elevated titers of these AAbs in cerebrospinal fluid correlate with manifestations of NPSLE within the CNS (8, 10, 18, 19). We have shown that NMDAR-reactive AAbs bind to the receptor by recognizing the 5-amino acid consensus sequence D/E W D/E Y S/G (DWEYS, for short) present in the NR2A and NR2B subunits (15). The DWEYS motif is localized in the extracellular, amino-terminal domain of NR2A (residues 283–287, sequence DWDYS) and NR2B (residues 284–288, sequence EWDYG) (20). Injection of murine or human monoclonal AAbs, with DWEYS specificity, into the hippocampus and cerebral cortex of mice results in local loss of neurons. Human AAbs with this specificity induce activation of caspase-3 in cultured human and murine neurons (15, 17).

We have used murine models to demonstrate a causal relationship between NMDAR-reactive AAbs and impairments in cognition and behavior (15, 17, 21–24). The proposal that NMDAR-reactive AAbs are causal agents for the symptoms of NPSLE must address the transit of AAbs from the blood into brain parenchyma. When mice are immunized with a multiantigenic peptide that consists of several copies of the DWEYS sequence multimerized on polylysine (MAP-DWEYS), the animals produce AAbs against DWEYS, dsDNA, and NMDAR. Surprisingly, even high serum titers of DWEYS-reactive AAbs do not elicit toxic effects in the brain. Intravenous injections of monoclonal AAbs are also innocuous to the brain. These negative results highlight the importance of the blood–brain barrier (BBB) in protecting the brain from exposure to potentially disruptive AAbs (23). Consequently, we have studied immunized mice after administration of agents that mimic in vivo events, such as inflammation and stress, which disrupt the BBB to allow penetration of circulating molecules into the brain. LPS is a bacterial component that induces inflammation and disturbs BBB integrity. Mice immunized with MAP-DWEYS and subsequently injected with LPS exhibited selective neuronal damage in the hippocampus (22). Epinephrine, which also disrupts the BBB, caused neuronal damage localized to the lateral amygdala in MAP-DWEYS immunized mice (21). Thus, the nature of the agent that impairs BBB integrity determines the brain region that will be affected by NMDAR-reactive AAbs. Behavioral assays in these animals have provided a reasonable model for the memory impairment and emotional disturbance observed in NPSLE.

Excitatory synaptic transmission occurs between glutamate-releasing presynaptic terminals and postsynaptic receptors such as NMDARs and amino-3-hydroxy-5-methylisoxazole-4-propionic

Author contributions: B.D. and P.T.H. designed research; T.W.F., E.H.C., C.K., R.B., E.B., and P.T.H. performed research; T.W.F., I.G.G., J.Z., J.S.-G., H.E.F.-L., and P.T.H. contributed new reagents/analytic tools; T.W.F., B.T.V., and P.T.H. analyzed data; and T.W.F., B.T.V., B.D., and P.T.H. wrote the paper.

The authors declare no conflict of interest.

*This Direct Submission article had a prearranged editor.

[1]To whom correspondence should be addressed. E-mail: pato.huerta@gmail.com.

This article contains supporting information online at www.pnas.org/lookup/suppl/doi:10.1073/pnas.1006980107/-/DCSupplemental.

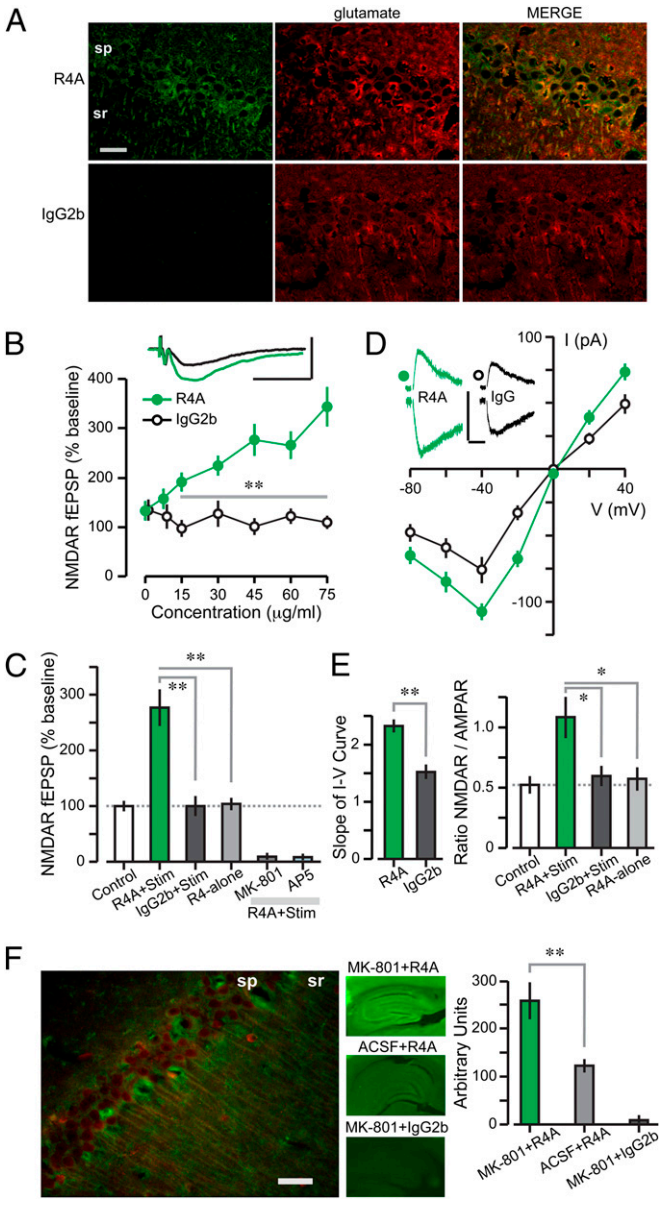

Fig. 1. NMDAR-reactive AAb, R4A, enhances the synaptic responses mediated by NMDARs. (*A*) Colocalization of R4A and glutamate labeling within CA1 pyramidal cells. (Scale bar: 20 μm.) (*B*) NMDAR-dependent fEPSPs (mean ± SEM) at rising concentrations of R4A and IgG2b (n = 10–12 per level) show a significant effect of R4A vs. IgG2b (F = 15.5, $P < 0.005$, ANOVA). Post hoc tests reveal that values >15 μg/mL are significantly different (**$P < 0.01$, t test). (*Inset*) Traces recorded after 10-min exposure to R4A (green, 45 μg/mL) or IgG2b (black, 45 μg/mL). [Scale bar: 0.5 mV (y axis), 50 ms.] (*C*) Graph shows that only R4A (45 μg/mL) coupled with synaptic stimulation (R4A+Stim, n = 10) enhances fEPSPs when compared with control (fEPSPs measured 5–10 min from onset of recording, without Ab addition); IgG2b (45 μg/mL, n = 10) or R4A-alone (45 μg/mL, n = 10) have null effects (R4A+Stim vs. IgG2b+Stim, T = 4.8; R4A+Stim vs. R4A-alone, T = 5.0; **$P < 0.001$, t test); fEPSPs are blocked by NMDAR inhibitors, MK-801 (50 μM, n = 8) or AP5 (100 μM, n = 8). (*D*) Current (I) to voltage (V) relations for NMDAR-dependent EPSCs (mean ± SEM) during R4A or IgG2b exposure (30 μg/mL each, n = 8–12 cells). (*Inset*), Sample EPSCs measured at +40 mV (*Upper*) and −40 mV (*Lower*). [Scale bar: 100 pA (y axis), 100 ms.] (*E*) (*Left*), Slope (mean ± SEM) of I-V curves (linear range, −40 to +40 mV) is significantly steeper for R4A-treated cells (30 μg/mL, T = 5.58, **$P < 0.001$, t test). (*Right*) N/A ratios (mean ± SEM) of NMDAR EPSC (at +40 mV) over AMPA EPSC (at −60 mV) tested for R4A and IgG2b (each at 45 μg/mL, n = 8–11 cells) show a significant enhancement for R4A-treated cells only (R4A+Stim vs. IgG2b+Stim, T = 2.6; R4A+Stim vs. R4A-alone, T = 2.7, *$P < 0.02$, t test). (*F*) (*Left*), CA1 pyramidal cells, after functional NMDAR blockade by MK-801 (as described in Fig. S1), show colocalized R4A and NR2A/B labeling in somata and dendrites. (Scale bar: 200 μm.) (*Middle*) Hippocampal sections stained with infrared-labeled Abs (R4A or IgG2b) are used to measure the strength of labeling. (*Right*) Graph shows strong R4A binding in sections pretreated with MK-801 (n = 8) and modest R4A binding in sections pretreated with artificial cerebral spinal fluid (n = 8, Z = 3.2, P = 0.0016, Mann–Whitney test); there is null IgG2b binding in MK-801-treated sections (n = 8). sp, *stratum pyramidale*; sr, *stratum radiatum*.

acid receptors (AMPARs). NMDARs are assembled with NR1, the essential channel-forming subunit that binds glycine and determines calcium permeability, and NR2 (A, B, C, and D) or NR3 (A and B) subunits that bind glutamate and regulate deactivation (25). When NMDARs work within the homeostatic range, they participate in synaptic plasticity (26) and activate cell survival-promoting cascades (27, 28). Conversely, prodeath signals emerge from NMDAR hypoactivity or hyperactivity (27, 28). The latter is marked by sustained rises in cytosolic calcium that accumulates excessively in organelles, especially mitochondria, resulting in depolarized mitochondrial membrane potential, lowered respiration, and increased production of reactive oxygen species (29). Following insult, mitochondria may either recover their membrane potential or undergo mitochondrial permeability transition (mPT), an irreversible collapse marked by an increase of inner membrane permeability and swelling, that is mediated by the formation of the mPT pore (30). Only a fraction of mitochondria needs to undergo mPT for apoptosis to occur (31). This event correlates with the release of proapoptotic factors and can be blocked by cyclosporine A (CSA), a potent mPT inhibitor (32, 33).

This study adapts the ex vivo hippocampal slice to explore AAb pathogenicity. This preparation allows us to preserve CA1 neurons as mature cells in a biologically relevant network, and permits the study of AAb neurotoxicity in an environment that may closely replicate the situation in vivo. We elucidate the cellular responses to varying concentrations of NMDAR-reactive AAbs and show that they function as modulators that amplify NMDAR-mediated synaptic signaling at low concentration and promote excitotoxicity through enhanced mitochondrial permeability transition at high concentration. Thus we provide a model for discrete CNS symptoms occurring as a function of Ab concentration.

Results

SLE AAbs Selectively Augment NMDAR-Mediated Synaptic Signaling. To study the effect of SLE AAbs within the microenvironment in which NMDAR activation and NPSLE occur, we used ex vivo hippocampal slices of female Balb/cJ mice (8–16 wk of age). We showed previously (15) that R4A, a murine monoclonal AAb cross-reactive with dsDNA and DWEYS, bound NMDARs in PC12 cells and caused neuronal death in vivo; therefore, we used R4A for modeling NMDAR-reactive AAbs and murine IgG2b as the isotype control Ab. We first determined, by immunocytochemistry, that R4A bound robustly to NMDAR-expressing cells in the CA1 region of the hippocampus; and that the R4A signal colocalized with the neurotransmitter glutamate in CA1 cells (Fig. 1*A*).

NMDAR-mediated synaptic responses were recorded as field excitatory postsynaptic potentials (fEPSPs) and excitatory postsynaptic currents (EPSCs) in CA1 (34). We studied NMDARs in pharmacological isolation by adding the appropriate blocking agents to the solution bathing the slice (NMDAR mixture in *SI Methods*). For each experiment, after establishing baseline synaptic responses (0.1 Hz stimulation, 10 min), the AAb was added for 10 min. R4A enhanced NMDAR-mediated fEPSPs in a concentration-dependent manner (Fig. 1*B*), and the NMDAR antagonists MK-801 (50 μM) or AP5 (50 μM) blocked this effect (Fig. 1*C*). Crucially, IgG2b failed to alter the fEPSPs (Fig. 1 *B* and *C*). Whole-cell recordings of CA1 cells revealed steeper current–voltage curves in cells treated with R4A (30 μg/mL), compared

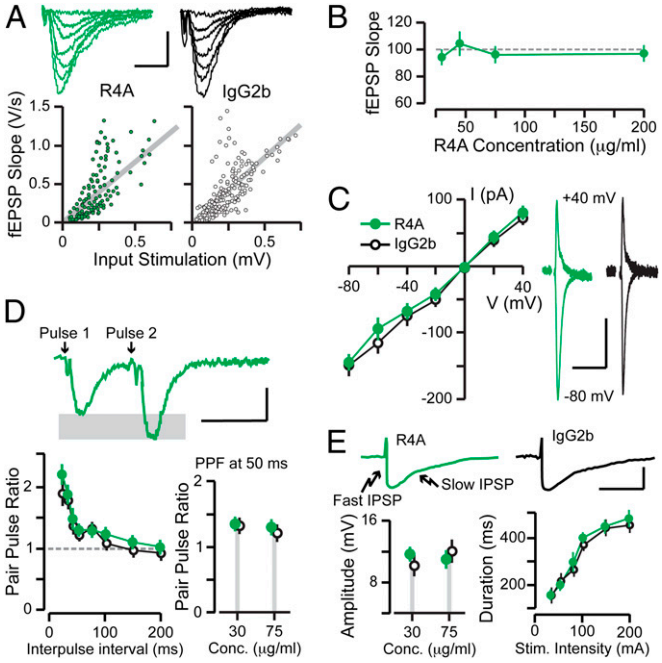

Fig. 2. Null effects of the NMDAR-reactive AAb, R4A, on AMPARs and GABARs. (*A*) (*Upper*) Traces correspond to AMPAR-mediated fEPSPs at increasing stimulation strengths. [Scale: 0.5 mV (*y* axis), 10 ms.] (*Lower*) Input–output functions measure AMPAR-mediated basal transmission. Each circle represents a single response. Gray lines indicate linear fits of the populations. There are no differences between R4A and IgG2b; each tested at 75 μg/mL. (*B*) Slope (mean ± SEM) of fEPSPs remains unchanged at rising R4A concentrations (n = 10–15 per level). (*C*) Current (I) to voltage (V) relations for AMPAR-mediated EPSCs (mean ± SEM), measured with whole-cell recordings, show that AMPAR transmission is unchanged by R4A (n = 9) compared with IgG2b (n = 7), each tested at 75 μg/mL. (*Right*) Sample EPSCs are shown at +40 mV and −80 mV. [Scale: 100 pA (*y* axis), 100 ms.] (*D*) Short-term plasticity is unaltered by R4A (n = 14) compared with IgG2b (n = 11), each tested at 75 μg/mL. (*Upper*) Sample fEPSPs from paired pulse stimulation. [Scale: 1 mV (*y* axis), 50 ms.] (*Lower Left*) Paired pulse profiles (mean ± SEM) at several intervals between pulses. (*Lower Right*) Plot of paired pulses ratios (mean ± SEM), at the 50-ms interpulse interval. (*E*) Inhibitory transmission is not affected by R4A (n = 8) compared with IgG2b (n = 7), each tested at 75 μg/mL. (*Upper*) Sample IPSPs illustrate the fast and slow components. [Scale: 100 mV (*y* axis), 200 ms.] (*Lower Left*) Plot of the peak amplitude (mean ± SEM) of the fast IPSP. (*Lower Right*) Profiles of slow IPSP duration (mean ± SEM) for increasing stimulation strengths.

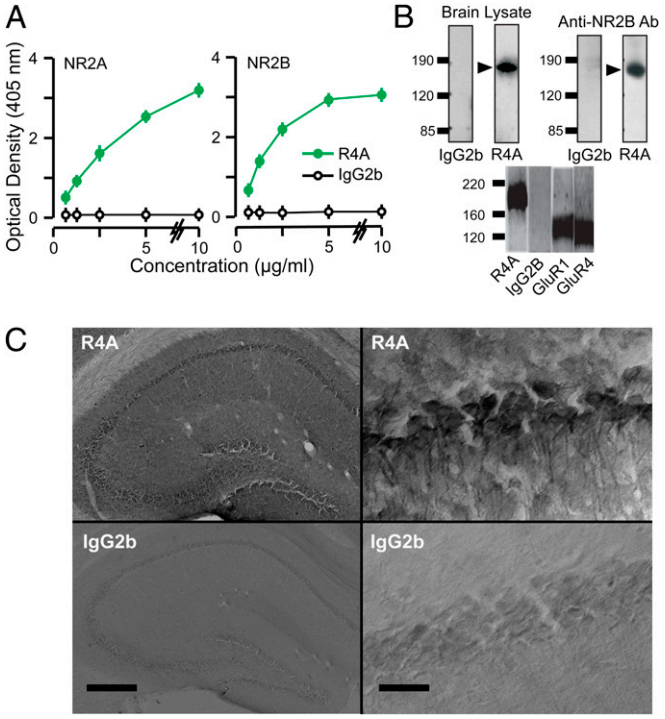

Fig. 3. Binding of the NMDAR-reactive AAb, R4A, to NMDARs. (*A*) Optical density values (mean ± SD), measured on ELISAs, for AAb binding to NR2A and NR2B. Increasing concentrations of R4A and IgG2b (n = 9 per level) are tested. ANOVAs reveal highly significant binding for R4A vs. IgG2b (NR2A, $F = 11.5$, $P < 0.005$; NR2B, $F = 18.5$, $P < 0.005$). (*B*) (*Upper Left*) Western blots of murine brain lysates are displayed on SDS/PAGE and probed with R4A and IgG2b. (*Upper Right*) Brain lysates are immunoprecipitated, with R4A and IgG2b, and probed with commercial Ab against NR2B. Numbers at left of gels indicate molecular weight; arrows mark molecular weight of NR2 subunits. (*Lower*) Brain lysates are immunoprecipitated with R4A, IgG2b, and Abs against GluR1 and GluR4, and displayed on SDS/PAGE. Bands for AMPAR subunits GluR1 and GluR4 do not coincide with R4A band. (*C*) (*Upper Left*) Robust binding of R4A in section of hippocampus treated with DNase and stained with R4A (60 μg/mL), followed by biotinylated secondary Ab. (*Upper Right*) R4A binds strongly to somata and dendrites of CA1 cells. (*Lower*) Sections stained with IgG2b (60 μg/mL) display null reactivity. (Scale bar on left: 500 μm; scale bar on right: 20 μm.) sp, *stratum pyramidale*; sr, *stratum radiatum*.

with IgG2b (30 μg/mL) (Fig. 1*D*). The N/A ratio (NMDAR-mediated EPSC at +40mV over AMPAR-mediated EPSC at −60mV, used for standardization between cells) was doubled during R4A (45 μg/mL) treatment as compared with untreated and IgG2b-treated cells (45 μg/mL) (Fig. 1*E*). Importantly, the addition of R4A (45 μg/mL) in the absence of synaptic activation resulted in unchanged NMDAR-mediated fEPSPs (Fig. 1*C*) and N/A ratios (Fig. 1*E*), when the values before R4A exposure were compared with those immediately after R4A washout, demonstrating that R4A by itself did not affect NMDARs. Thus, we showed that R4A acted selectively as a positive modulator that enhanced the NMDAR responses triggered by glutamate.

The failure of R4A to alter the NMDAR-mediated responses in the absence of synaptic stimulation suggested that R4A preferentially interacted with open NMDAR channels. To assess this possibility, we reasoned that MK-801 (irreversible blocker of synaptic NMDARs; Fig. S1), applied during synaptic activation, may stabilize the NMDAR pore in its open-state configurations (35). Therefore, slices were treated with MK-801 (50 μM) during strong stimulation, fixed, cut into thin sections (30–40 μm), and stained with R4A or IgG2b. R4A displayed approximately twofold greater binding to slices that were pretreated with MK-801 than to nontreated slices and colocalized with NR2A/B; IgG2b bound neither tissue (Fig. 1*F* and Fig. S2). We thus concluded that R4A exhibited preferential binding to the open pore of the NMDAR.

To confirm the functional selectivity of NMDAR-reactive AAbs, we examined other neurotransmitter systems that might possibly be affected by the AAbs. We studied AMPARs by isolating them pharmacologically (36) with the appropriate blocking agents (AMPAR mixture described in *SI Methods*). We found that AMPAR-mediated fEPSPs and EPSCs were unaffected by R4A even at a high AAb dose (200 μg/mL) (Fig. 2 *A* and *B*). In addition, we studied inhibitory postsynaptic potentials (IPSPs), mediated by receptors for γ-amino-butyric acid of the A type (GABAaRs) and the B type (GABAbRs). To accomplish this, we modified the mixture of blocking agents (GABAR mixture described in *SI Methods*). R4A had no effect on the IPSPs that were mediated by GABAaRs and GABAbRs (Fig. 2*C*). Presynaptic function was examined with the paradigm of paired pulse facilitation (36). This phenomenon was not altered in the presence of R4A (Fig. 2*D*). Thus, we showed

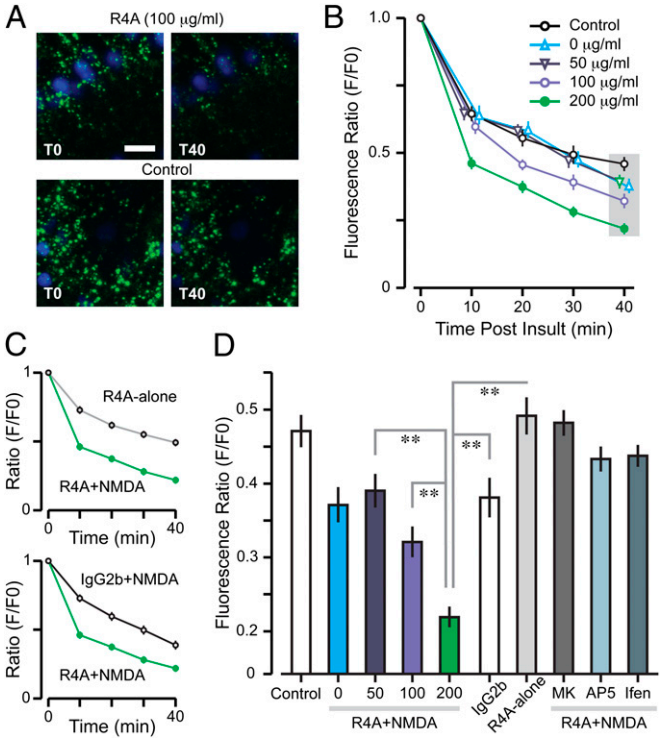

Fig. 4. NMDAR-reactive AAb, R4A, increases mPT. (*A*) CA1 neurons with cell bodies stained by DAPI (blue). Calcein-loaded mitochondria (green) occur in somata and dendrites of CA1 cells. (*Upper*) R4A (200 μg/mL) coapplied with NMDA (10 mM) leads to a marked attenuation of mitochondrial fluorescence, demonstrating mPT. (*Lower*) Control refers to a condition in the absence of NMDA and R4A, showing only minor decay in fluorescence. (Scale bar: 10 μm.) T0, onset of insult; T40, 40 min after insult. (*B*) Decay profiles (mean ± SD) for calcein fluorescence during coapplication of NMDA (10 mM) and R4A (0–200 μg/mL). ANOVAs for control vs. R4A, with time as repeated measure, reveal differences for the high-dose groups (100 μg/mL, $F = 28.8$, $P < 0.01$; 200 μg/mL, $F = 21.1$, $P < 0.01$). (*C*) (*Upper*) Decay profile (mean ± SD) for R4A (200 μg/mL) coapplied with NMDA (10 mM) is significantly different from R4A-alone (ANOVA with time as repeated measure, $F = 25$, $P < 0.001$). (*Lower*) R4A+NMDA is also significantly different from IgG2b (200 μg/mL) coapplied with NMDA (ANOVA with time as repeated measure, $F = 14.2$, $P < 0.01$). (*D*) Graph shows fluorescence ratios plotted at T40 (indicated by gray area in *B*). Incremental mPT occurs at increasing levels of R4A+NMDA (50 vs. 200 μg/mL, $T = 5.6$; 100 vs. 200 μg/mL, $T = 4.1$; $^{**}P < 0.001$, *t* test). Ratio for R4A at 200 μg/mL is significantly lower than R4A-alone ($T = 9.6$, $^{**}P < 0.001$, *t* test) and IgG2b+NMDA ($T = 5.8$, $^{**}P < 0.001$, *t* test). NMDAR inhibitors MK-801 (100 μM), AP5 (2.5 mM), and ifenprodil (10 μM) completely block mPT when coapplied with R4A (200 μg/mL) and NMDA (10 mM).

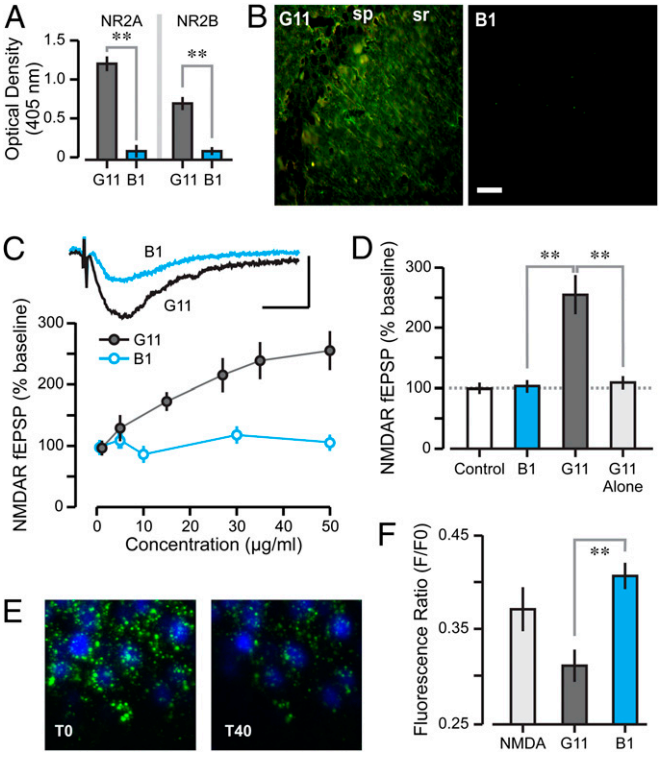

Fig. 5. Human NMDAR-reactive AAb, G11, binds NMDARs, enhances NMDAR-mediated synaptic responses and augments mPT. (*A*) Optical density values (mean ± SD), measured on ELISAs, for binding of G11 (5 μg/mL, $n = 12$) and control Ab B1 (5 μg/mL, $n = 12$) to NR2A and NR2B. Student *t* tests reveal significant binding for G11 vs. B1 (NR2A, $T = 8.2$; NR2B, $T = 5.2$; $^{**}P < 0.001$). (*B*) CA1 neurons treated with DNase and stained with G11 and B1 (each at 10 μg/mL) followed by FITC-conjugated secondary Ab; G11 section is also stained with Ab against glutamate. (Scale bar: 20 μm.) sp, *stratum pyramidale*; sr, *stratum radiatum*. (*C*) Graph shows NMDAR-mediated fEPSPs (mean ± SEM) at increasing concentrations of G11 and B1 ($n = 10$–12 per level). ANOVA reveals a significant concentration effect for G11 vs. B1 ($F = 9.8$, $P < 0.05$). (*Inset*) Traces recorded after 10-min exposure of G11 or B1 (each at 50 μg/mL). [Scale bar: 0.5 mV (*y* axis), 50 ms.] (*D*) Graph (mean ± SEM) shows enhancement of NMDAR-mediated fEPSPs by G11 (50 μg/mL, $n = 12$), null effect of the innocuous Ab, B1 (50 μg/mL, $n = 10$), and lack of enhancement by G11 in the absence of synaptic stimulation (G11-alone, $n = 10$). Student *t* tests reveal significant differences (B1 vs. G11, $T = 4.7$; G11 vs. G11-alone $T = 4.2$; $^{**}P < 0.01$). (*E*) Sample fields of CA1 before (T0) and 40 min after (T40) treatment with NMDA and G11. (Scale bar: 10 μm.) (*F*) Decrease in calcein fluorescence at T40, expressed as F/F0 ratios (mean ± SD). Notice the clear mPT amplification in the G11 group. B1 fails to enhance mPT (B1 vs. G11, $T = 4.4$, $^{**}P < 0.001$, *t* test).

that R4A had a null effect on other receptors within the CA1 region and would enhance but not initiate NMDAR activation.

SLE AAbs Bind to NMDARs. A clear specificity of R4A for the NMDAR was established by using ELISAs, Western blots, and immunoprecipitation assays (Fig. 3 *A* and *B*). ELISAs were performed on recombinant, extracellular domains of NR2A and NR2B, ensuring that the DWEYS epitope was well exposed. R4A bound both subunits in a dose-dependent manner, whereas mouse IgG2b showed null binding (Fig. 3*A*). We next determined the binding of NMDAR-reactive AAbs to native NMDARs by immunocytochemistry. Because R4A could react with dsDNA, we treated the brain sections with DNase to reduce DNA reactivity. Immunostaining with R4A revealed strong binding to CA1 cells (Fig. 3*C*). Notably, the R4A signal colocalized with glutamate (Fig. 1*A*) and NR2A/B within CA1 cells (Fig. S3). Crucially, the control IgG2b failed to show binding to NMDARs (Fig. 1*A* and 3*C*). Collectively, these results showed that R4A reacted specifically with the NR2A and NR2B subunits, in their native and denatured states.

SLE AAbs at High Concentration Augment mPT. We monitored mPT as a key indicator for AAb-triggered cellular stress and excitotoxicity by adapting the calcein–cobalt [II] (Co^{2+}) method for imaging mPT (37, 38) to hippocampal slices (Fig. S4). The agonist NMDA (10 mM) activated NMDARs and produced a slight increase in mPT (Fig. S5); thus, we coapplied R4A with NMDA and found that R4A produced a dose-dependent amplification of NMDA-induced mPT (Fig. 4), consistent with R4A binding NMDARs that were already activated. Interestingly, a significantly higher R4A concentration was required to induce mPT (100 μg/mL) than to enhance NMDAR-mediated fEPSPs (15 μg/mL). This effect was blocked by AP5 as well as ifenprodil (NR2B-specific antagonist); IgG2b had no effect (Fig. 4*D*). In the absence of NMDA, R4A did not amplify the baseline mPT (Fig. 4*D*).

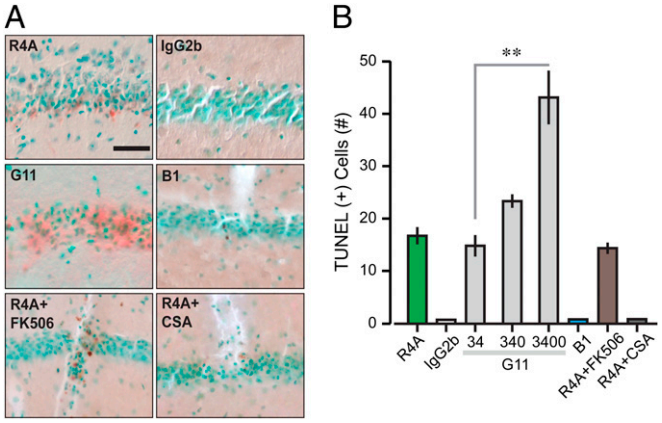

Fig. 6. NMDAR-reactive AAbs produce apoptosis in vivo, mediated by mPT. (*A*) Micrographs of *stratum pyramidale* in CA1, stained with TUNEL, reveal apoptotic nuclei (brown) against methyl-green background. (Scale bar: 50 μm.) Injections of R4A (18 μg/mL) and G11 (34 μg/mL) result in TUNEL(+) cells, whereas injections of IgG2b (18 μg/mL) and B1 (34 μg/mL) have null effects. Coinjection of R4A (18 μg/mL) with FK506 (10 μM) shows lack of protection of this specific calcineurin inhibitor. However, coinjection with CSA (10 μM) reveals protection by CSA (which inhibits both cyclophilin D and calcineurin). Thus, mPT is involved in the apoptotic effect. (*B*) Graph shows the quantification of AAb-induced apoptosis (n = 5–8 sections per group). TUNEL(+) cells are measured in a volume (1.5×10^6 μm^3) centered around the injection site. Notice that G11 is probed at increasing doses (34, 340 and 3,400 μg/mL). There is a significant concentration-dependent effect of G11 on apoptosis (34 vs. 3,400 μg/mL, Z = 2.7, P = 0.006, Mann–Whitney test).

Human NMDAR-Reactive AAbs Enhance NMDAR-Mediated fEPSPs and mPT. We wanted to ascertain whether human SLE AAbs were modulators of the NMDAR, as shown for the murine AAb R4A. We tested G11, a monoclonal AAb that was cloned from peripheral blood B cells of a SLE patient, which displayed reactivity to NMDARs, dsDNA, and DWEYS (39). As a control, we used B1, an isotype control human monoclonal Ab that did not react with dsDNA or NMDARs (39). ELISAs with recombinant extracellular domains of NR2A and NR2B showed that G11 bound both subunits, whereas murine B1 showed null binding (Fig. 5*A*). Immunocytochemical assessment showed that, like R4A, G11 bound excitatory pyramidal cells in CA1 (Fig. 5*B*); the control B1 displayed null binding (Fig. 5*B*). Electrophysiological experiments showed that, like R4A, G11 elicited a dose-dependent increase of NMDAR-mediated fEPSPs in CA1 synapses, whereas B1 had no effect (Fig. 5*C*). We also tested whether G11 was efficacious in the absence of synaptic stimulation and found that, immediately after exposure to G11 (45 μg/mL), the sizes of NMDAR-mediated fEPSPs were similar to those before AAb treatment (Fig. 5*D*). These results indicated that G11 functioned as a positive NMDAR modulator in the same manner as R4A. We further demonstrated that the similarities in mechanism between murine and human AAbs carried over to effects on mPT. G11 (200 μg/mL) was capable of amplifying the NMDA-induced mPT, whereas the control B1 (200 μg/mL) was not (Fig. 5 *E* and *F*). Again, a significantly higher concentration of human AAb was necessary to induce mPT than to augment NMDAR-mediated fEPSPs.

NMDAR-Reactive AAbs Cause Apoptosis Through mPT. We sought to verify whether the neurotoxicity of NMDAR-reactive AAbs in vivo (15) occurred through increased mPT. Therefore, we injected AAbs directly into CA1 and, 24 h later, performed TUNEL on fixed sections to identify apoptotic nuclei. R4A and G11 injections, but not IgG2b and B1, produced clear apoptosis (Fig. 6). We used CSA to check whether cyclophilin D (a crucial component of the mPT) was involved in the AAb-mediated apoptotic pathway. Because CSA inhibits calcineurin as well as cyclophilin D, we also tested a specific calcineurin blocker, FK506. Coinjection of R4A with CSA prevented apoptosis, while coinjection with FK506 failed to provide a neuroprotective effect, demonstrating that cyclophilin D contributes to AAb-mediated apoptosis (Fig. 6).

High Concentrations of NMDAR-Reactive AAbs Are Present in SLE CSF. We wanted to know whether sufficient AAb was present in CSF of SLE patients to mediate either synaptic changes or excitotoxicity. We therefore generated a standard curve for IgG binding to the DWEYS peptide, with the use of peptide-affinity purified Abs derived from the serum of three SLE patients. This procedure allowed us to address the variability in IgG subclass and affinity present in polyclonal responses. We used DWEYS reactivity as a surrogate for NMDAR reactivity. The concentration of this AAb in the CSF of patients with CNS manifestations of NPSLE ranged from 10 μg/mL to >300 μg/mL (Fig. 7), indicating that the levels of NMDAR-reactive AAbs present in the patient's CSF might result in synaptic alteration and mitochondrial dysfunction.

Discussion

Our study represents a unique effort to adapt the adult hippocampal slice preparation to explore the AAb pathogenicity. Preserving the state of CA1 neurons as mature cells, in a biologically relevant network, allows the study of AAb neurotoxicity in an environment that may closely replicate the in vivo situation. We show here that the NMDAR-reactive AAbs, R4A and G11, function as modulators that preferentially bind to the open NMDAR pore and function only on neurons with activated synapses. Thus, AAb binding probably increases the open-state duration, a function that is regulated by glutamate (35). We also demonstrate that pathogenic SLE AAbs require a higher titer, or higher activity, to induce neuronal stress than to induce electrophysiological changes in NMDAR-mediated synaptic transmission. This may mirror the condition of NPSLE patients, in which transient changes may reflect synaptic effects, whereas permanent damage may reflect neurotoxicity. In addition, the effects of differential AAb titer, and access to brain, may cause severe episodes in some NPSLE patients in which substantial neuronal death occurs, whereas in other NPSLE patients symptoms may be reversible. We, and others, have shown that AAb titer in CSF determines the nature and severity of NPSLE (9, 16–19). Moreover, the severity of the cognitive impairment following intrauterine exposure to AAb is directly correlated with AAb titer (24). The fact that the range of concentrations of NMDAR-reactive AAb in the CSF of patients with CNS manifestations of NPSLE falls within the AAb range used in this study strongly implies that the concentrations present in CSF might alter synaptic function only or might also mediate neuronal death.

Our study provides mechanistic insights into the neuronal dysfunction mediated by AAbs in SLE. During NPSLE episodes, the AAbs might cause short-term changes but, alternatively, might cause more long-lasting degeneration. After a critical loss of neurons, there may be further neuronal death that progresses through nonimmunological pathways. Our results also illustrate how there can be both reversible and irreversible effects of AAb

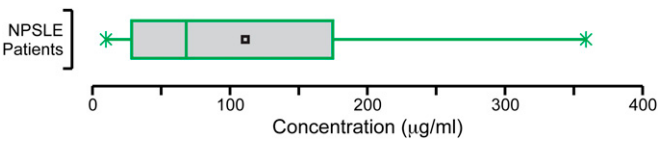

Fig. 7. Range of NMDAR-reactive AAbs in CSF. Box plot shows NMDAR-reactive AAbs in CSF obtained from 32 patients with NPSLE. DWEYS-reactive IgGs are assayed by ELISA, and concentrations are then determined with a standard curve generated from peptide-specific IgG (affinity-purified from sera of three patients with SLE). Obs., observations.

exposure, providing a model for distinct outcomes of Ab exposure depending solely on Ab concentration. This observation also suggests that these AAbs, potentially dangerous in SLE patients, may be harnessed for therapeutic use in instances of inadequate NMDAR function (21).

Methods

Animals. Female Balb/cJ mice (Jackson Laboratory) were housed in groups (five animals per cage) and maintained on a 12-h light/dark cycle with food and water available ad libitum. Animals were 8–16 wk old when used for the experimental procedures, which were performed in accordance with National Institutes of Health guidelines. The Institutional Animal Care and Use Committees of Weill Cornell Medical College and the Feinstein Medical Research Institute approved the animal protocols.

Electrophysiology. The procedures for the preparation of ex vivo slices from the hippocampus and the electrophysiological measurement of synaptic responses (34, 36), while applying AAbs, are detailed in *SI Methods*.

Immunocytochemistry. The techniques for immunostaining hippocampal tissue with SLE AAbs, colabeling with commercial Abs (against of L-glutamate and against NR2A/B), and for assaying TUNEL(+) cells are detailed in *SI Methods*.

Biochemical Assays. ELISAs were performed as described previously (22), using 5 μg/mL of the recombinant external domains of NR2A or NR2B (550-aa long) for coating the plate and the indicated concentration of AAbs (Fig. 3*A*). Western blot was done using 20–60 μg of membrane-enriched brain lysate from brains of adult BALB/cJ mice snap frozen in liquid nitrogen. R4A was used at 2.5 μg/mL for direct binding and 10 μg/mL for immunoprecipitation. Anti-NR2B Ab (A6474, Invitrogen) was used at 1 μg/mL.

Quantification of AAb in Human CSF. A standard curve was generated from DWEYS-reactive IgG that had been affinity purified from serum of SLE patients (n = 3) on a peptide column. The standard curve was used to calculate the concentration of DWEYS-reactive IgG in the CSF of 32 patients with NPSLE (8).

Confocal Live Imaging of mPT. We developed a unique procedure for imaging mitochondrial stress in brain neurons within *ex vivo* slices. The implementation of the calcein–cobalt [II] (Co^{2+}) method to monitor mPT (38, 39) is described in Figs. S4 and S5 and *SI Methods*.

Statistical Analysis. Data are presented as mean ± SEM, or mean ± SD, as indicated. We used factorial ANOVA, repeated measures ANOVA, the Student t test, and the Mann–Whitney test to examine statistical significance, which was defined as $P < 0.05$.

ACKNOWLEDGMENTS. We thank Kelvin K. Chan and Scott Hayes for experimental help and Tomás S. Huerta for comments on the manuscript. E.H.C. is a Goldsmith Research Fellow at Burke Cornell Medical Research Institute. This work was supported by National Institutes of Health Program Grant 5P01AI073693-02 (to B.D., P.T.H., and B.T.V.).

1. Lahita RG (1995) Special report: Adjusted lupus prevalence. Results of a marketing study by the Lupus Foundation of America. *Lupus* 4:450–453.
2. Lahita RG (2004) *Systemic Lupus Erythematosus* (Elsevier, Amsterdam), 4th Ed.
3. Hochberg MC (1997) Updating the American College of Rheumatology revised criteria for the classification of systemic lupus erythematosus. *Arthritis Rheum* 40:1725.
4. Tan EM, et al. (1982) The 1982 revised criteria for the classification of systemic lupus erythematosus. *Arthritis Rheum* 25:1271–1277.
5. Brey RL, et al. (2002) Neuropsychiatric syndromes in lupus: Prevalence using standardized definitions. *Neurology* 58:1214–1220.
6. Hanly JG (2005) Neuropsychiatric lupus. *Rheum Dis Clin North Am* 31:273–298, vi.
7. Kozora E, Hanly JG, Lapteva L, Filley CM (2008) Cognitive dysfunction in systemic lupus erythematosus: Past, present, and future. *Arthritis Rheum* 58:3286–3298.
8. Fragoso-Loyo H, et al. (2008) Serum and cerebrospinal fluid autoantibodies in patients with neuropsychiatric lupus erythematosus. Implications for diagnosis and pathogenesis. *PLoS ONE*, 10.1371/journal.pone.0003347.
9. Hanly JG, Robichaud J, Fisk JD (2006) Anti-NR2 glutamate receptor antibodies and cognitive function in systemic lupus erythematosus. *J Rheumatol* 33:1553–1558.
10. Husebye ES, et al. (2005) Autoantibodies to a NR2A peptide of the glutamate/NMDA receptor in sera of patients with systemic lupus erythematosus. *Ann Rheum Dis* 64: 1210–1213.
11. Lapteva L, et al. (2006) Anti-N-methyl-D-aspartate receptor antibodies, cognitive dysfunction, and depression in systemic lupus erythematosus. *Arthritis Rheum* 54:2505–2514.
12. Omdal R, et al. (2005) Neuropsychiatric disturbances in SLE are associated with antibodies against NMDA receptors. *Eur J Neurol* 12:392–398.
13. Steup-Beekman G, Steens S, van Buchem M, Huizinga T (2007) Anti-NMDA receptor autoantibodies in patients with systemic lupus erythematosus and their first-degree relatives. *Lupus* 16:329–334.
14. Yoshio T, Onda K, Nara H, Minota S (2006) Association of IgG anti-NR2 glutamate receptor antibodies in cerebrospinal fluid with neuropsychiatric systemic lupus erythematosus. *Arthritis Rheum* 54:675–678.
15. DeGiorgio LA, et al. (2001) A subset of lupus anti-DNA antibodies cross-reacts with the NR2 glutamate receptor in systemic lupus erythematosus. *Nat Med* 7:1189–1193.
16. Emmer BJ, van der Grond J, Steup-Beekman GM, Huizinga TW, van Buchem MA (2006) Selective involvement of the amygdala in systemic lupus erythematosus. *PLoS Med*, 10.1371/journal.pmed.0030499.
17. Kowal C, et al. (2006) Human lupus autoantibodies against NMDA receptors mediate cognitive impairment. *Proc Natl Acad Sci USA* 103:19854–19859.
18. Yoshio T, Okamoto H, Minota S (2007) Antibodies to bovine serum albumin do not affect the results of enzyme-linked immunosorbent assays for IgG anti-NR2 glutamate receptor antibodies: Reply to the letter by Hirohata et al. *Arthritis Rheum* 56:2813–2814.
19. Arinuma Y, Yanagida T, Hirohata S (2008) Association of cerebrospinal fluid anti-NR2 glutamate receptor antibodies with diffuse neuropsychiatric systemic lupus erythematosus. *Arthritis Rheum* 58:1130–1135.
20. Gielen M, Siegler Retchless B, Mony L, Johnson JW, Paoletti P (2009) Mechanism of differential control of NMDA receptor activity by NR2 subunits. *Nature* 459:703–707.
21. Diamond B, Huerta PT, Mina-Osorio P, Kowal C, Volpe BT (2009) Losing your nerves? Maybe it's the antibodies. *Nat Rev Immunol* 9:449–456.
22. Kowal C, et al. (2004) Cognition and immunity; antibody impairs memory. *Immunity* 21:179–188.
23. Huerta PT, Kowal C, DeGiorgio LA, Volpe BT, Diamond B (2006) Immunity and behavior: Antibodies alter emotion. *Proc Natl Acad Sci USA* 103:678–683.
24. Lee JY, et al. (2009) Neurotoxic autoantibodies mediate congenital cortical impairment of offspring in maternal lupus. *Nat Med* 15:91–96.
25. Cull-Candy SG, Leszkiewicz DN (2004) Role of distinct NMDA receptor subtypes at central synapses. *Sci STKE* 2004:re16.
26. Bliss TV, Collingridge G, Morris RM (2007) *The Hippocampus Book*, eds Andersen P, Morris RM, Amaral D, Bliss TV, O'Keefe J (Oxford University Press, Oxford), pp 343–474.
27. Hardingham GE, Bading H (2003) The Yin and Yang of NMDA receptor signalling. *Trends Neurosci* 26:81–89.
28. Martel MA, Wyllie DJ, Hardingham GE (2009) In developing hippocampal neurons, NR2B-containing N-methyl-D-aspartate receptors (NMDARs) can mediate signaling to neuronal survival and synaptic potentiation, as well as neuronal death. *Neuroscience* 158:334–343.
29. Schinder AF, Olson EC, Spitzer NC, Montal M (1996) Mitochondrial dysfunction is a primary event in glutamate neurotoxicity. *J Neurosci* 16:6125–6133.
30. Abramov AY, Duchen MR (2008) Mechanisms underlying the loss of mitochondrial membrane potential in glutamate excitotoxicity. *Biochim Biophys Acta* 1777:953–964.
31. Pivovarova NB, et al. (2004) Excitotoxic calcium overload in a subpopulation of mitochondria triggers delayed death in hippocampal neurons. *J Neurosci* 24:5611–5622.
32. Brustovetsky N, Brustovetsky T, Jemmerson R, Dubinsky JM (2002) Calcium-induced cytochrome c release from CNS mitochondria is associated with the permeability transition and rupture of the outer membrane. *J Neurochem* 80:207–218.
33. Shalbuyeva N, Brustovetsky T, Bolshakov A, Brustovetsky N (2006) Calcium-dependent spontaneously reversible remodeling of brain mitochondria. *J Biol Chem* 281: 37547–37558.
34. Chang EH, et al. (2006) AMPA receptor downscaling at the onset of Alzheimer's disease pathology in double knockin mice. *Proc Natl Acad Sci USA* 103:3410–3415.
35. Kussius CL, Popescu GK (2009) Kinetic basis of partial agonism at NMDA receptors. *Nat Neurosci* 12:1114–1120.
36. Chang EH, Rigotti A, Huerta PT (2009) Age-related influence of the HDL receptor SR-BI on synaptic plasticity and cognition. *Neurobiol Aging* 30:407–419.
37. Petronilli V, et al. (1999) Transient and long-lasting openings of the mitochondrial permeability transition pore can be monitored directly in intact cells by changes in mitochondrial calcein fluorescence. *Biophys J* 76:725–734.
38. Gillessen T, Grasshoff C, Szinicz L (2002) Mitochondrial permeability transition can be directly monitored in living neurons. *Biomed Pharmacother* 56:186–193.
39. Zhang J, et al. (2008) Identification of DNA-reactive B cells in patients with systemic lupus erythematosus. *J Immunol Methods* 338:79–84.